Noise Prediction of an Open Fan Using Acoustic Analogy Approaches

Masakazu Sugiyama, Fabrice Falissard, Gabriel Reboul, Nassim Jaouani, Xavier Gloerfelt

Noise Prediction of an Open Fan Using Acoustic Analogy Approaches

Masakazu Sugiyama[1*], **Fabrice Falissard**[**], **Gabriel Reboul**[***], **Nassim Jaouani**[*] **and Xavier Gloerfelt**[****]

[*]Safran Aircraft Engines - Rond-Point René Ravaud, Réau 77550 Moissy-cramayel, France

[**]DAAA, ONERA, Université Paris Saclay, F-92190 Meudon - France

[***]DAAA, ONERA, Université Paris Saclay, F-92322 Châtillon, France

[****]École Nationale Supérieure d'Arts et Métiers (ENSAM) - 151, boulevard de l'hôpital, 75013 Paris, France

ABSTRACT

The purpose of this study is to evaluate numerical aero-acoustic methods for the noise prediction of an open fan, which is expected to reduce CO_2 emissions for the next generation of aircraft engines. The far-field noise is computed using a CFD/CAA approach. The unsteady Reynolds Averaged Navier-Stokes (uRANS) and the Ffowcs Williams-Hawkings (FWH) analogy using solid and permeable surfaces are applied. The phase-lag method (single-blade passage) is used for the purpose of calculation for aerodynamic flow and noise sources with ONERA elsA finite volume solver. The sensitivities to the numerical CFD setup as well as the position and formulation of FWH permeable surface for noise computation are discussed in this paper. The present noise prediction strategy is evaluated for approach and take-off operating conditions. In particular, several spatial discretization schemes and FWH surface locations are tested and compared to evaluate their influence on the noise levels and directivity.

1. INTRODUCTION

Engine manufacturers are enhancing the efficiency of aircraft engines to reduce their environmental impact, for which a 20% CO_2 reduction is expected [1], to be achieved by increasing fan's bypass ratio. Notably, mechanical simplicity makes the Open Fan a more attractive choice than CROR (Contra-Rotating Open Rotor). It consists of rotating "rotors" and fixed "stators", such as depicted in figure 1. Considering stricter regulations year after year, reducing noise became also one of key challenges. State of the art methodologies for noise prediction rely on the use of CFD (Computational Fluid Dynamics) and acoustic analogy based on the Ffowcs Williams and Hawkings (FWH) equation. In the same way that high-accuracy simulations are needed for hybrid predictions of jet noise [2, 3], great care to numerical setup must be taken to ensure the same level of accuracy for Open Fan noise prediction. For instance, several approaches have been presented using the hybrid CFD-FWH method [4–8]. In particular, these papers including the studies of jet noise prediction suggest that the shape of FWH's permeable surface as well as its location play a crucial role for the prediction of the level and directivity. Moreover, there is not yet consensus on closing or not the permeable surface downstream of the jet as well as the wake of the open rotor.

In the present paper, the results of application of the uRANS-FWH method for Open Fan configuration at 2 flight conditions are discussed. The numerical approach will be detailed in section 3. Different numerical spatial schemes are tested to quantify their influence on acoustic noise prediction. Finally, the sensitivity of type and shape of FWH surface is then evaluated for assessing the ability of FWH method to predict Open Fan noise radiation.

[1]masakazu.sugiyama@safrangroup.com

2. GEOMETRY AND OPERATING CONDITION

The Open Fan geometry used in this paper consists of N_r rotor blades and N_s stator blades and, as already stated, only the rotor part rotates in a counterclockwise direction. A simplified hub is also employed and extended in the downstream direction as an infinite cylindrical hub. Two operating conditions are considered. The first one is an approach condition at a freestream Mach number of 0.22 and rotor rotation speed of approximately 600 rpm. The second operating condition is a take-off condition at Mach number of 0.29, in which rotation speed is close to 1000 rpm. These parameters are summarized in Table 1.

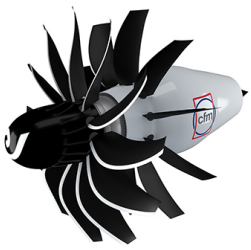

Figure 1: Example of Open Fan [1]

Table 1: Description of the two operating conditions

	Approach	**Take-off**
Flight Mach number M_∞	0.22	0.29
Rotation speed $[rpm]$	600.0	1000.0
Angle of attack $[deg]$	0.0	0.0

3. NUMERICAL APPROACH

In this section, the numerical method for Open Fan aerodynamic and acoustic calculations is presented. First, a RANS calculation is carried out with the ONERA's elsA finite solver [9] applying a mixing plane approximation. The mixing plane is an interface between the rotor and the stator grids, where each rotor outlet boundary and stator inlet boundary is calculated respectively from each zone and averaged circumferentially as steady-state. The RANS solution is used as the initial condition for the uRANS computation. The unsteady simulation accounts only for a single rotor and stator blade channel and relies on a phase-lag approach (shown in figure 2). Finally, unsteady blade pressures are used for FWH solid surfaces formulation, or unsteady aerodynamic fields are used for the FWH permeable surface formulation in order to compute the noise radiated in the far-field using ONERA's KIM solver [10]. More details are given in the following section.

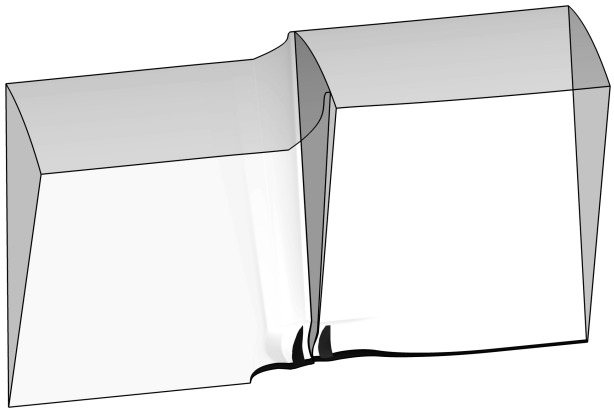

Figure 2: CFD computation domain using phase-lag method

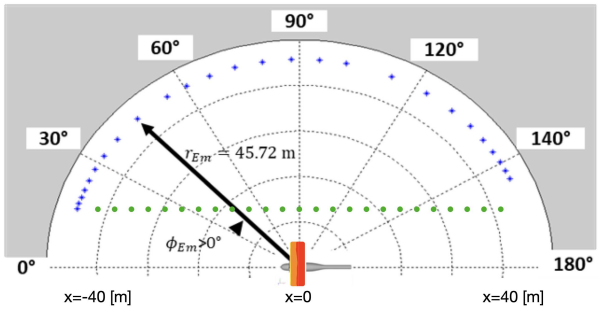

Figure 3: Microphones position with the pressure contour on FWH permeable surfaces
blue dots : spherical, green dots : linear

3.1. Computational Grid

The computation grid is generated in structural multi-block form by the commercial mesher Autogrid. Our mesh strategy must meet two requirements. Firstly, the Y+ value on the blade surface is always set less than 1, so the surface mesh as well as the mesh layers around the surface are quite refined. Secondly, the grid expands up to reaching the mesh size corresponding to 20 points per wavelength corresponding to the first harmonic of the Blade Passing Frequency (BPF) in the axial and azimuthal directions. This size is kept constant up to 4 times the rotor radius. This strategy leads to 25M cells for the lower Mach condition (approach) and 36M cells for the higher Mach condition (take-off).

3.2. Phase-lag approach

The phase-lag approach enables computation of an unsteady flow in rotational stages using only a single channel but as if calculated with a whole rotational domain, which was primarily introduced by Erdos *et al* [11] and is generally called "chorochronic" approach. Taking the periodicity of flow between stages into account, the idea of this technique is to treat flow states in each single space (choro) and time (chronic) of a single channel, which is "recycled" for neighbor's flow states computation according to the periodicity. A reconstruction for a whole 360 deg domain is then indispensable so that it is not a simple duplication, but an interpolation of space information to mesh grid at each time step. Then, the noise radiation in the far-field from the aerodynamic information, which is reconstructed for 360 deg domain, is computed with ONERA's KIM solver. Although the phase-lag approach has some drawbacks such as the omission of information due to the simplification, it has been attractive for CROR's acoustic prediction in many papers [6, 12, 13] due to its ease of handling and good cost performance.

3.3. Numerical set-up

The CFD computations are carried out using the cell-centered volume finite solver elsA [9] developed at ONERA (ONERA-Safran property), solving the Reynolds-averaged Navier-Stokes equations for aerodynamic flow prediction of Open Fan's single-channel domain. The k-ω Wilcox [14] is chosen for the RANS model. Several spatial schemes are tested to examine their influences on aerodynamic but also acoustic predictions. Firstly, a second-order centered Jameson's scheme [15] with the scalar artificial viscosity is chosen as a reference case. Two upwind schemes, Roe scheme [16] and an AUSM+ scheme for low-Mach number flow [17, 18] , are also applied, with spatial order accuracy varying between 3rd and 5th order by means of MUSCL reconstruction [19]. The Roe scheme is a flux difference scheme (FDS), in which jacobian fluxes with Roe-averages are used for the dissipation flux evaluation. On the other hand, the AUSM scheme is a flux vector splitting scheme (FVS) because the mass flux part is split with the velocity or Mach number. The temporal scheme used for the RANS calculation is a first-order backward scheme, while for the unsteady simulation, a three time level implicit backward difference formula is employed. A far-field condition is imposed on external boundaries and the mixing plane condition is imposed at the interface between rotor and stator section as mentioned above for steady state calculations. Besides, an adiabatic wall condition is set for blade and hub surfaces.

3.4. Acoustic computation

The acoustic calculation based on FWH's integral method takes place with the ONERA's KIM solver. After the uRANS calculation and the reconstruction described in the section **3.2**, the noise source on complete FWH's surfaces is propagated using both the FWH's impermeable surface and the permeable surface formulations using the free-field convected Green function. The FWH's formulations applied in this paper are detailed in [10]. With regard to FWH's solid surface, only rotor and stator blades are evaluated and the noise contribution from the nacelle surface is not considered. The FWH permeable approach uses arbitrary surfaces surrounding the rotor & stator flow domains.

An example is shown in figure 3 with the microphones location. Two microphone placements are used, a spherical and a linear microphone placement, properly. Each practice has 8 polar lines in the azimuthal direction with the same number of microphones. It enables to consider an average when performing the noise computation. The acoustic sensitivity to the position of FWH's permeable surface is investigated. For this study, 5 different permeable surfaces are tested. The upstream surface for all cases is located at 1.4R (R;radius) in the radial direction and at 0.25R upstream to rotor and ends up at different positions downstream. The 1st to 4th surfaces are closed at different downstream locations, 0.7R, 2R, 3R and 4R respectively. The 5th one is an opened cylindrical surface, which is not closed downstream but ends at the 4R from the rotor. The different FWH's permeable surfaces are shown in figure 4 and summarized in table 2. It should be noted that all surfaces are located within the refined grid, which was defined in Section 3.1.

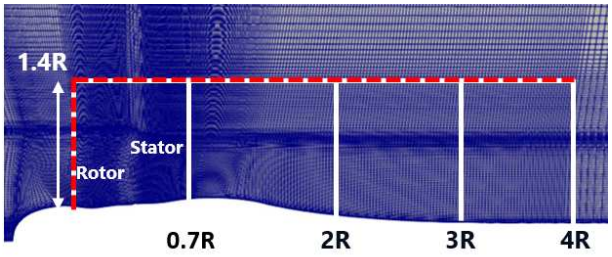

Figure 4: FWH's permeable surface description with CFD mesh

Table 2: FWH's permeable surface position

	Abbreviation	Closure position
Surface 1	S1	0.7R
Surface 2	S2	2R
Surface 3	S3	3R
Surface 4	S4	4R
Surface 5	S5	opened (4R)

4. RESULTS

In the following sections, the aerodynamic performances as well as acoustic results for the Open Fan are presented.

4.1. Aerodynamic performance

First of all, the aerodynamic performances with the RANS simulations employing the mixing plane approach are compared for the various spatial schemes presented in section **3**. The power coefficient C_P and the thrust coefficient C_T are compared. The results are normalized and evaluated by taking the Jameson scheme as a reference case. The C_P and the C_T are computed with $C_P = P/\rho_\infty n^3 D^5$ and $C_T = T/\rho_\infty n^2 D^4$ respectively, where P and T are the power and the thrust generated by the rotor. n represents the rotation frequency and D is defined as the rotor diameter. Table 3 and table 4 show the results for the different spatial schemes for the approach and the take-off conditions. Clearly, only slight differences are found for both C_P and C_T between numerical schemes. Pressure coefficient C_p on the rotor blade section at 0.75R in the spanwise direction on the rotor surface is then plotted for the approach condition in figure 5. All curves are almost perfectly superimposed, so we conclude that, in terms of aerodynamic performance, the influence of spatial scheme, regardless of their order, is negligible.

4.2. Wake analysis

Next, the flow wake generated by the rotor blade is analyzed. The same various schemes are tested for the approach point. Figure 6 and 7 represent the vorticity magnitude isocontours in a Y-plane and the turbulence intensity at the plane in front of the mixing plane, respectively. Figure 6 shows the vorticity produced by the rotors reaching the leading edge of the stators. As figure 7, higher the order of scheme is, more the turbulence intensity is emphasized due to better spatial resolution with lower

	C_P	Δ[%]	C_T	Δ[%]
Jameson (ref. case)	1.0000	0.00	1.0000	0.00
Roe O(3)	1.0004	0.04	1.0000	0.00
AUSM O3	1.0004	0.04	1.0000	0.00
Roe O(5)	1.0004	0.04	1.0000	0.00
AUSM O5	1.0023	0.23	1.0044	0.44

Table 3: Approach operating point aerodynamic performances

	C_P	Δ[%]	C_T	Δ[%]
Jameson (ref. case)	1.0000	0.00	1.0000	0.00
Roe O(3)	1.0007	0.07	1.0031	0.31
AUSM O3	1.0015	0.15	1.0003	0.03

Table 4: Take-Off operating point aerodynamic performances

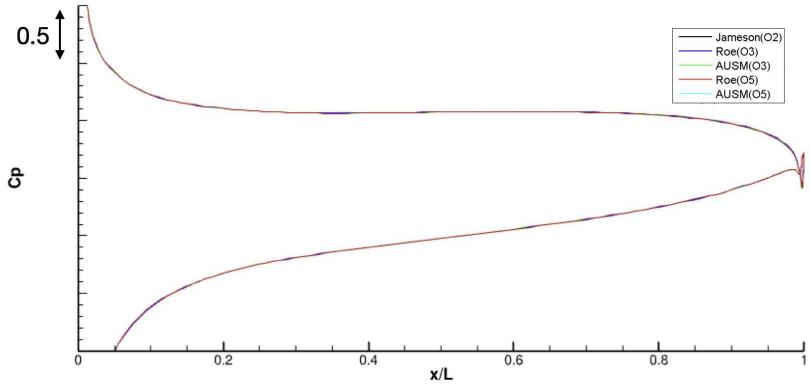

Figure 5: Pressure coefficient on rotor at 0.75R

numerical dissipation. Unexpectedly, the Roe **O**(3) scheme is the least evaluated but the maximum value produced by the tip vortex of rotor, is as high as Jameson scheme. The Roe **O**(5) and the AUSM+ **O**(5) schemes give almost identical results along the spanwise and the AUSM+ **O**(3) lies between them. These outcomes suggest that the order of numerical scheme does not impact on the steady aerodynamic characteristics but on the wake flow unsteadiness, which may affect the acoustic performances. As mentioned in [20], the viscous wake or the tip vortex interaction [12,21,22] between the rotors plays a vital role for the tone noise and the broadband noise for the CROR configuration. Mostly the same noise source mechanisms can apply for the Open Fan configuration. So, resolving the interaction between the rotor and the stator with further precision would matter for Open Fan noise computation.

4.3. Sensitivity of FWH formulation type

The noise results will now be quantified. Primarily, the sensitivity of FWH formulation type, solid and permeable for the acoustic is discussed. Figure 8 shows the SPL for 1-3 $\times$ BPF and OASPL (OverAll Sound-Pressure Level) results with the Jameson scheme for both FWH formulations at the approach point. The linear microphone placement (green dotted line in figure 3) is used in this test. Both figures have the same Y-range and the observer location is represented in x-axis, the same hereinafter. Here, the opened surface S5 is used for FWH permeable formulation. FWH solid formulation has tendency to underestimate SPL, except for upstream direction, compared to permeable one. A difference comes from the fact that a permeable formulation takes into account the quadrupolar sources. This underestimation indicates that the flow is strongly non uniform within the permeable surface even in the approach operating condition where the blade loading is small. Moreover, the noise directivity

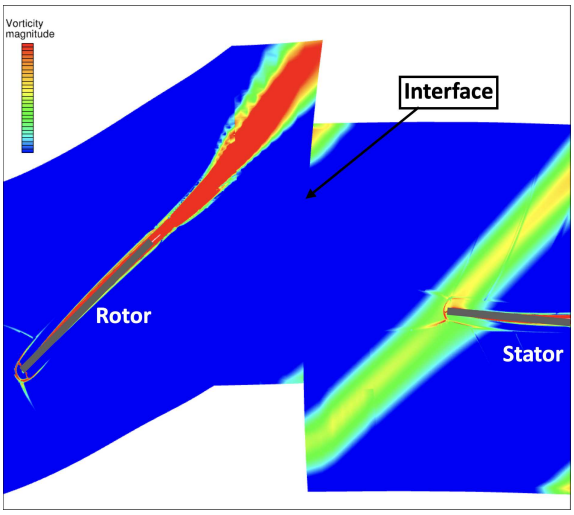

Figure 6: Vorticity magnitude (s^{-1}) isocontour with the chorochronic method

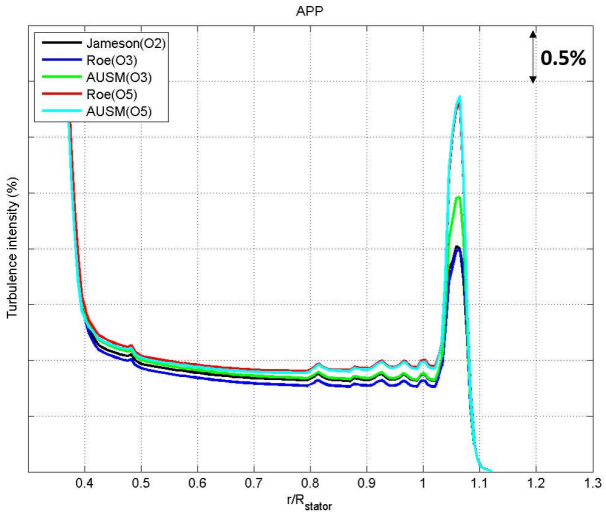

Figure 7: Turbulence intensity (%) in the front vicinity of the mixing plane

shift in the upstream direction around $x = -15m$ is observed. An explanation to this shift counts on the underlying assumption developed in FWH method that the acoustic waves propagate in an uniform flow. The lack of complex propagation effects can influence the results of the solid surface formulation.

4.4. Influence of spatial scheme on the acoustic

The effect of numerical scheme on acoustics is then discussed in this section for the approach operating point. The opened permeable surface S5 (red dashed line in figure 4) as well as FWH solid surfaces are still considered. The spherical microphone placement (blue dotted line in figure 3) is used for noise computation. Figure 9 displays the far-field OASPL. The results for both solid and permeable surfaces show the variation of OASPL in the upstream and downstream directions while the peak value has almost the same level between schemes. Remarkably, a 5dB discrepancy between the Jameson scheme (**O**(2)) and the 5th order schemes is observed in the upstream direction $\theta < 40°$ for the permeable surface results. 2-3dB difference appears also for the solid surface results. This gap is similar to the gap on the turbulence intensity, shown in figure 7. For low Mach number condition with low blade thrust, the impingement of rotor blade viscous wake on stator blades (figure 6) is the main contributor to interaction noise so that increasing the spatial accuracy of the numerical scheme has a sensible impact on the emitted noise. Furthermore, the mesh fineness in the wake zone can be responsible for the generation of pseudo-sound, as noted in the paper [2].

4.5. Sensitivity of FWH permeable closure surface position

The objective of this final section is to study the sensitivity of FWH's surface position. The tested surfaces are already described in figure 4 and in table 2 in section **3.4**. The numerical scheme is always the 2nd order centered scheme. The linear microphone array used again. The comparison of SPL for 1-3 $\times$ BPF as well as OASPL versus the observer x-position is plotted as a solid line in figure 10 and in figure 11 for the approach and take-off conditions. The acoustic results in the two regimes depend strictly on whether and where the downstream surface closes, nevertheless, the maximum of SPL is not sensitive to the closure location. The SPL variates in the upstream and downstream direction for the approach case, while strong influences appear only in the downstream direction for the take-off case. Several reasons arise. First, spurious noise can be generated as the wake crosses the FWH control surface, as reported in [23]. This spurious noise is often called the hydrodynamic effect noise [24]. In practice, figure 10 shows that, by moving the closure surface away from the Open Fan,

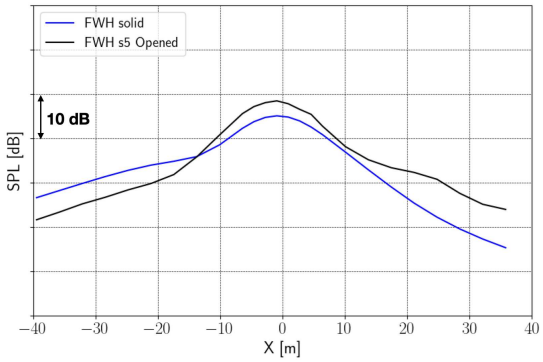

(a) SPL vs. Observer position on x for 1 × BPF

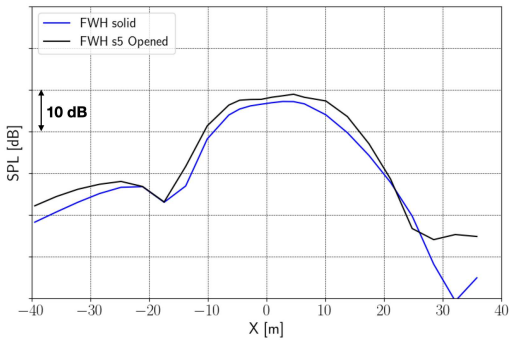

(b) SPL vs. Observer position on x for 2 × BPF

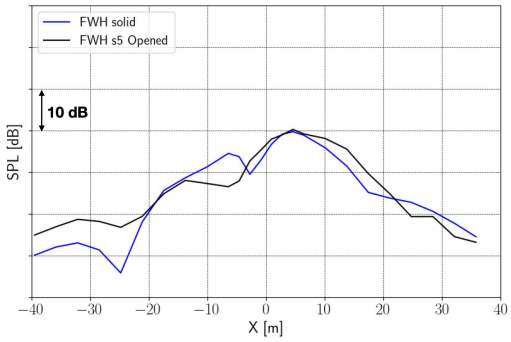

(c) SPL vs. Observer position on x for 3 × BPF

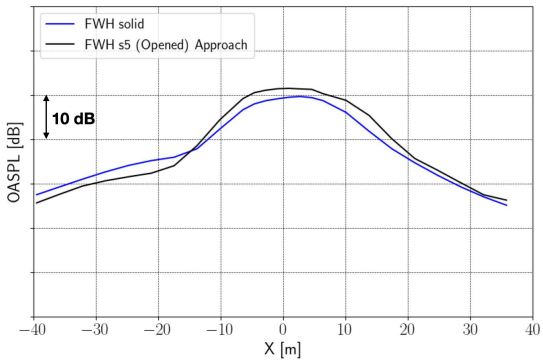

(d) OASPL vs. Observer position on x for all BPF

Figure 8: Sound pressure level for approach with Jameson scheme

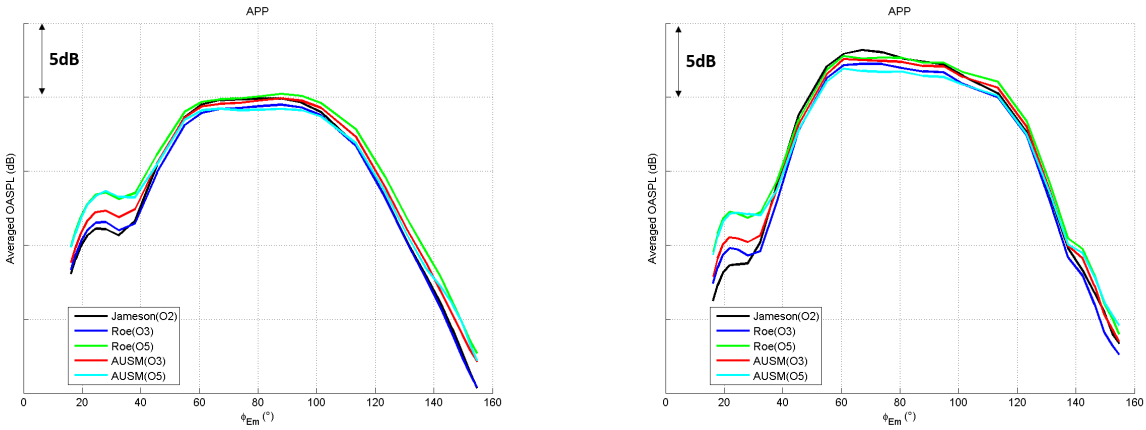

(a) FWH solid surface OASPL vs. Observer polar angle

(b) FWH permeable surface (opened) OASPL vs. Observer polar angle

Figure 9: Effect of numerical scheme on noise levels for the approach operating point

the results of the closed surface have a tendency to converge to the opened surface S5's result. The second reason is due to the refraction produced by the blowing of the rotors as presented in [4, 7]. Thirdly, it could be due to the pseudo-sound generated by the mesh coarsening as mentioned in the previous section.

So, we focus now on the spurious noise effect. The KIM solver allows to diminish the contribution of hydrodynamic fluctuations to the spurious noise by adding a source term [23]. The results with the additional term correction are added as dashed lines in figures 10 and 11. Actually, the additional term correction attenuates the impact of FWH closure location. Especially, the correction works well for the upstream direction at take-Off condition, where the vortex intensity is expected to be stronger than the approach condition. The additional term does not act much in the downstream direction nor in the upstream direction at approach condition. These results are consistent with the results observed for jet noise simulations reported in [23].

5. CONCLUSIONS

An aero-acoustic methodology for the Open Fan noise prediction has been investigated through this paper. The CFD computations were conducted with the use of the phase-lag approach and the noise radiation was calculated using FWH's acoustic analogy. Several spatial schemes and FWH applications were tested to evaluate their effects on the aerodynamic performances but also on the far-field noise prediction.

This study showed the importance of resolution of viscous wake and choice of FWH formulation. The primary cause of Open Fan's noise in approach condition is due to the interaction of the rotor wake with the stator. It is essential to pay attention to the order of the numerical scheme to capture properly aerodynamic noise sources. Even at low-Mach number condition, the flow is highly non-uniform close to the rotor and stator, which promotes the use of FWH permeable surface for the Open Fan noise prediction. The shape of the FWH permeable surface and its closure position have strong impact on the noise directivity prediction. Each shape and closure locations have advantages and drawbacks, the additional correction term being helpful in mitigating the spurious noise due to the hydrodynamic fluctuations. Another way to reduce the influence of the permeable surface definition would be to refine the grid furthermore.

This paper revealed characteristics of noise prediction for Open Fan with the CFD/FWH hybrid application. Current perspectives and further issues on the methodology are to deepen the study of the interaction between numerical resolution and acoustic predictions, and also to validate the prediction with wind-tunnel measurements.

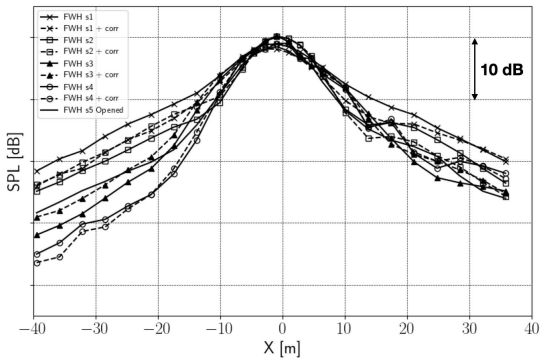

(a) SPL vs. Observer position on x for 1 × BPF

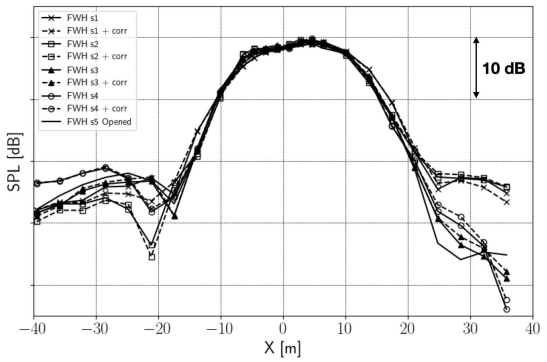

(b) SPL vs. Observer position on x for 2 × BPF

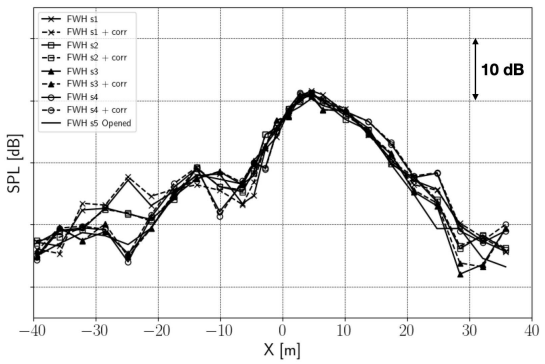

(c) SPL vs. Observer position on x for 3 × BPF

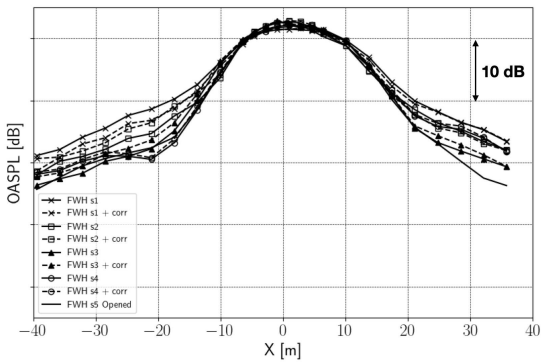

(d) OASPL vs. Observer position on x for all BPF

Figure 10: Sensitivity to the outlet closure position of FWH permeable surface for the approach condition

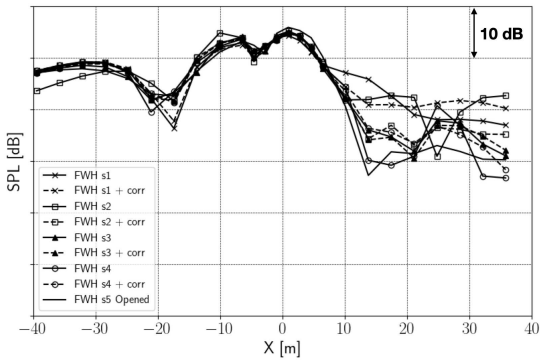

(a) SPL vs. Observer position on x for 1 × BPF

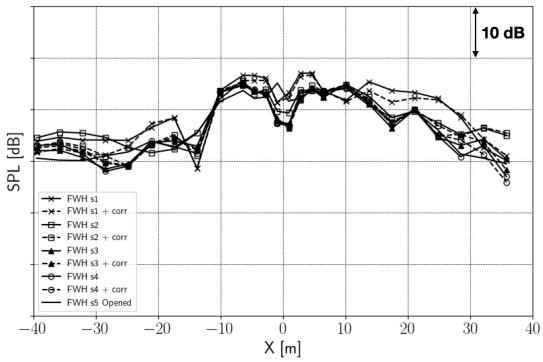

(b) SPL vs. Observer position on x for 2 × BPF

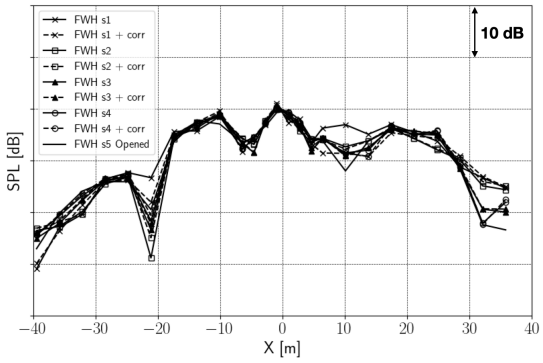

(c) SPL vs. Observer position on x for 3 × BPF

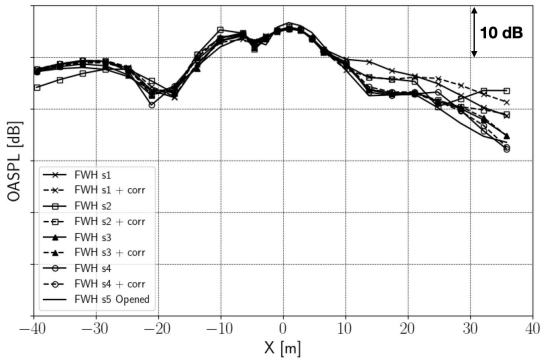

(d) OASPL vs. Observer position on x for all BPF

Figure 11: Sensitivity to the outlet closure position of FWH permeable surface for the take-Off condition

ACKNOWLEDGEMENTS

This work was conducted within the Safran-ONERA research program MONICA. The authors would like to acknowledge the French civil aviation directorate (DGAC) for supporting this project. The calculations were performed at Safran Aircraft Engines and ONERA using their computer resources. The authors thank Jean Michel Lucas, Jacky Mardjono, Vincent Dayde-Thomas (Safran Aircraft Engines) and Jean-Christophe Boniface (DAAA/ONERA) for sharing their experiences and discussions. We are grateful to Safran Aircraft Engines Acoustic Design team, especially, Ryad Bellot, Thomas Riboulet and Eric Tran for helping with CFD calculations.

REFERENCES

1. CFM. CFM RISE program. https://www.cfmaeroengines.com/rise/. Last accessed 2023-04-10.
2. P. R. Spalart M. L. Shur and M. Kh. Strelets. Noise prediction for increasingly complex jets. Part I: Methods and tests. Part II: Applications. *International Journal of Aeroacoustics*, Vol. 4((3+4)):213–266, 2005.
3. G. Rahier O. Labbé, C. Peyret and M. Huet. A CFD/CAA coupling method applied to jet noise prediciton. *Computers and Fluids*, Vol.86:1–13, 2013.
4. M. L. Shur P. R. Spalart, A. K. Travin and M. Kh. Strelets. Initial noise predictions for open rotors using first principles. *AIAA paper 2010-3793*, 2010.
5. Y. Colin, A. Carazo, B. Caruelle, T. Nodé-Langlois and A. B. Perry . Computational strategy for predicting CROR noise at low-speed part I: Review of the numerical methods. *AIAA paper 2012-2221*, 2012.
6. Y. Colin, F. Blanc, B. Caruelle, T. Nodé-Langlois and A. B. Perry. Computational strategy for predicting CROR noise at low-speed part II: investigation of the noise sources comp. *AIAA paper 2012-2222*, 2012.
7. B. Caruelle Y. Colin and A. B. Perry. Computational strategy for predicting CROR noise at low-speed III: investigation of noise radiation with the Ffowcs-Williams Hawkings analogy. *AIAA paper 2012-2223*, 2012.
8. Y. Colin, B. Caruelle,T. Nodé-Langlois, M.Omais, P.Spiegel and A. B. Perry. Installation effects on contra-rotating open rotor noise at high-speed. *AIAA paper 2014-2971*, 2014.
9. L. Cambier, S. Heib and S.Plot. The ONERA elsA CFD software: input from research and feedback from industry. *Mechanics and Industry*, 14(3):159–174, 2013.
10. J. Prieur and G. Rahier. Aeroacoustic integral methods, formulation and efficient numerical implementation. *Aerospace Science and Technology*, 5(7):457–468, 2001.
11. J.I. Erdos, E. Alzner and W. Mc Nally. Numerical solution of periodic transonic flow through a fan stage. *AIAA J.*, 15(11):1559–1568, 1977.
12. G. Delattre and F. Falissard. Influence of torque ratio on counter-rotating open-rotor interaction noise. *AIAA J.*, 53(9):2726–2738, 2015.
13. F. Falissard, R. Boisard, R. Gaveriaux, G. Delattre, P. Gardarein, A. Chelius, S. Canard-Caruana and Y. Maufrey. Influence of blade deformations on open-rotor low-speed and high-speed aerodynamics and aeroacoustics. *AIAA paper 2017-3869*, 2017.
14. D.C. Wilcox. Formulation of the k-ω turbulence model revisited. *AIAA J.*, 46(11):2823–2838, 2008.
15. A. Jameson. Origins and further development of the Jameson–Schmidt–Turkel scheme. *AIAA paper 2015-2718*, 2015.

16. P.L. Roe. The use of the Riemann problem in finite difference schemes. *Lecture Notes in Physics, 141, Proceedings of the 7th International Conference on Numerical Methods in Fluid Dynamics, Springer-Verlag*, 1980.
17. M.S. Liou. A Sequel to AUSM: AUSM+. *Journal of Computational Physics*, 129(0256):364–382, 1996.
18. I. Mary and P. Sagaut. Large eddy simulation of flow around an airfoil near stall. *AIAA J.*, 40(6), 2002.
19. B. van Leer. Toward the ultimate conservative difference scheme.IV. A new approach to numerical convection. *Journal of Computational Physics*, 23:276–299, 1977.
20. S. Moreau and M. Roger. Advanced noise modeling for future propulsion systems. *International Journal of Aeroacoustic*, 17(6-8):576–599, 2018.
21. P. Zehner, F. Falissard and X. Gloerfelt. Aeroacoustic study of the interaction of a rotating blade with a Batchelor vortex. *AIAA J.*, 56(2):629–647, 2018.
22. P. Zehner, F. Falissard and X. Gloerfelt. Vortex model and blade span influence on orthogonal blade-vortex interaction noise. *AIAA J.*, 58(8):3405–3413, 2020.
23. G. Rahier, M. Huet and J. Prieur. Additional terms for the use of Ffowcs Williams and Hawkings surface integrals in turbulent flows. *Computers and Fluids*, 120:158–172, 2015.
24. P. R. Spalart, K. V. Belyaev, M. L. Shur, M. Kh. Strelets and A. K. Travin. On the difference in noise predictions based on solid and permeable surface Ffowcs Williams-Hawkings integral solutions. *International Journal of Aeroacoustics*, 18((6-7)):621–646, 2019.